https://doi.org/10.5194/egusphere-2022-923
Preprint. Discussion started: 4 October 2022

Mapping of ESA-CCI land cover data to plant functional types for use in the CLASSIC land model

Libo Wang[1], Vivek K. Arora[2], Paul Bartlett[1], Ed Chan[1], and Salvatore R. Curasi[34]

[1]Climate Processes Section, Climate Research Division, Environment and Climate Change Canada, Toronto, ON, Canada

[2]Canadian Centre for Climate Modelling and Analysis, Climate Research Division, Environment and Climate Change Canada, Victoria, BC, Canada

[3]Department of Geography and Environmental Studies, Carleton University, Ottawa, ON, Canada.

[4]Climate Processes Section, Climate Research Division, Environment and Climate Change Canada, Victoria, BC, Canada.

Corresponding author: Libo Wang, Libo.Wang@ec.gc.ca

https://doi.org/10.5194/egusphere-2022-923
Preprint. Discussion started: 4 October 2022

Abstract

Plant functional types (PFTs) are used to represent vegetation distribution in land surface models (LSMs). Large differences are found in the geographical distribution of PFTs currently used in various LSMs. These differences arise from the differences in the underlying land cover products but also the methods used to map or reclassify land cover data to the PFTs that a given LSM represents. There are large uncertainties associated with existing PFT mapping methods since they are largely based on expert judgment and therefore are subjective. In this study, we propose a new approach to inform the mapping or the cross-walking process using analyses from sub-pixel fractional error matrices, which allows for a quantitative assessment of the fractional composition of the land cover categories in a dataset. We use the Climate Change Initiative (CCI) land cover product produced by the European Space Agency (ESA). A previous study has shown that compared to fine-resolution maps over Canada, the ESA-CCI product provides an improved land cover distribution compared to that from the GLC2000 dataset currently used in the CLASSIC (Canadian Land Surface Scheme Including Biogeochemical Cycles) model. A tree cover fraction dataset and a fine-resolution land cover map over Canada are used to compute the sub-pixel fractional composition of the land cover classes in ESA-CCI, which is then used to create a cross-walking table for mapping the ESA-CCI land cover categories to nine PFTs represented in the CLASSIC model. There are large differences between the new PFTs and those currently used in the model. Offline simulations performed with the CLASSIC model using the ESA-CCI based PFTs show improved winter albedo compared to that based on the GLC2000 dataset. This emphasizes the importance of accurate representation of vegetation distribution for realistic simulation of surface albedo in LSMs. Results in this study suggest that the sub-pixel

https://doi.org/10.5194/egusphere-2022-923
Preprint. Discussion started: 4 October 2022

fractional composition analyses are an effective way to reduce uncertainties in the PFT mapping process and therefore, to some extent, objectify the otherwise subjective process.

1. Introduction

Land cover is a critical component of the earth system that affects the exchange of energy, water, and carbon between the land surface and the atmosphere (Pielke et al., 1998; Sterling et al., 2013). Accurate representation of global land cover (LC) is important for land surface models (LSMs) which provide the lower boundary conditions to the atmosphere in weather forecast, climate, and earth system models. Plant functional types (PFTs) are groups of plant species that share similar structural, phenological, and physiological traits, and have been used in LSMs to represent vegetation distribution. This is because it is far more challenging to model biogeochemical processes, especially photosynthesis and the carbon cycle, at the species level (Bonan et al., 2002; Smith et al., 1997). The number and type of PFTs used in each LSM differ. Global LC datasets are typically used to derive the fractional coverage and geographical distribution of PFTs for use in LSMs. However, large differences exist in fractional coverage and geographical distribution of PFTs, which are caused by differences in the LC datasets themselves but also due to the methods used to map LC datasets to the PFTs represented in various models (Fritz et al, 2011; Hartley et al., 2017; Ottle et al., 2013; Wang et al., 2016).

Since different PFTs are characterized by different physical and biogeochemical processes and parameter values, the spatial distribution and fractional cover of PFTs constitute one of the important geophysical fields that are required for realistic simulation of carbon, water, and energy budgets in LSMs (Arora and Boer, 2010; Betts, 2001). For example, the surface albedos

https://doi.org/10.5194/egusphere-2022-923
Preprint. Discussion started: 4 October 2022

for needleleaf evergreen trees, broadleaf deciduous trees, and grasslands are very different, especially during winter when deciduous trees are leafless and short vegetation is largely buried by snow (Bartlett and Verseghy, 2015; Moody et al., 2007). Surface roughness for short or tall vegetation is also very different, which affects simulated turbulent exchanges. Wang et al. (2016) found that the bias in winter albedo in selected boreal forest regions among the models participating in the fifth phase of the Coupled Model Intercomparison Project (CMIP5) was largely related to bias in leaf area index and tree cover fraction. Model experiments using the MPI-ESM by Georgievski and Hagemann (2019) suggested that uncertainties in vegetation distribution may lead to noticeable variations in near-surface climate variables and large-scale circulation patterns.

The Canadian Land Surface Scheme Including Biogeochemical Cycles (CLASSIC) is an open-source community land model that is designed to address research questions that explore the role of the land surface in the global climate system (Melton et al., 2020). It is the successor to the coupled modelling framework based on the Canadian Land Surface Scheme (CLASS; Verseghy, 1991; 1993) and the Canadian Terrestrial Ecosystem Model (CTEM; Arora and Boer, 2005; Melton and Arora, 2016). The physics and biogeochemistry modules of CLASSIC are based on CLASS and CTEM models, respectively. Since the development of CTEM in the early 2000s, the GLC2000 LC product has been used to specify the spatial distribution of PFTs for CLASSIC when employed as the land surface component of the Canadian Earth system model developed by Environment and Climate Change Canada (Arora et al., 2009; Wang et al., 2006). The Climate Change Initiative (CCI) LC product recently produced by the European Space Agency (ESA) is available at an annual temporal resolution for the period 1992 to 2018 at 300 m spatial resolution (ESA, 2017). It was produced based on broad user consultation, specifically to address

https://doi.org/10.5194/egusphere-2022-923
Preprint. Discussion started: 4 October 2022

the needs of the climate modelling community (Bontemps et al., 2012). Wang et al. (2019) showed that when compared to the finer resolution maps over Canada, the 300 m ESA-CCI product provides much improved LC distribution over Canada compared to that from the 1 km GLC2000 dataset.

To map LC classes to PFTs, a cross-walking table (CW-table) is usually created to assign fractions of each LC class to the different PFTs, such that the sum of the fractions for each class is always one (including fractions of water and bare ground). Previous methods for creating such CW-tables are mainly based on LC class descriptions, expert knowledge, and the spatial distribution of global biomes (Ottle et al., 2013; Poulter et al., 2011; 2015; Sun and Liang, 2007; Wang et al., 2006). Because LC maps only provide the types of vegetation, and each class can be associated with a broad range of fractional cover of either one or more vegetation types, there are large uncertainties associated with any cross-walking or reclassification process. Wang et al. (2019) reclassified the 10 PFTs in the default CW-table provided in the ESA-CCI LC product user manual (Table 7-2, ESA, 2017) into four broad PFTs in CLASS, and compared them with those based on the GLC2000 dataset. The results suggest that uncertainties in the CW-tables were a major source of large differences in the PFT distributions. In addition, the fractional coverage of tree PFTs based on the default CW-table for the ESA-CCI LC dataset was overestimated along the taiga-tundra transition zone in western Canada, which led to underestimation in winter albedo in CLASSIC offline simulations driven with observation-based reanalysis data (Wang et al., 2018).

The objective of this study is to develop a new CW-table for reclassifying the ESA-CCI LC classes into PFTs used in the CLASSIC model for use over the model's Canada domain and to compare and assess the performance of CLASSIC offline simulations using the new and existing

https://doi.org/10.5194/egusphere-2022-923
Preprint. Discussion started: 4 October 2022

PFTs. Given the close link between the bias in winter albedo and the vegetation distribution in the models (Wang et al., 2016), our assessment of model performance focuses on the simulated surface albedo during the maximum snow accumulation period (February–March for the boreal forest). This simplifies our analyses by excluding the fall/spring transition periods when biases in snow accumulation and melt timing can have a large influence on surface albedo simulated by LSMs (Wang et al., 2014). In addition, we extend the CW-table for the ESA-CCI LC dataset to the global domain. A comprehensive assessment of the impact of the PFT distribution based on the new CW-table and the ESA-CCI LC dataset on the performance of the CLASSIC model at the global scale is presented in Arora et al. (2022).

2. Data and the CLASSIC model

2.1 The Hybrid LC map over Canada

The open access to the United States Geological Survey archive of Landsat imagery has provided free access to georeferenced and spectrally analysis-ready imagery (Wulder et al., 2012), which makes it possible to generate time series of LC maps to study LC change. Recently two of these products based on Landsat imagery are generated over Canada, including the North America Land Change Monitoring System (NALCMS) LC dataset (Latifovic et al., 2017) and the Virtual Land Cover Engine (VLCE) framework-generated LC dataset (Hermosilla et al., 2018).

Based on the random forest algorithm and local optimization method, the Canada Centre for Remote Sensing has generated LC maps of Canada for the years 2010 and 2015 at 30 m resolution using Landsat imagery (Latifovic et al., 2017). These LC products are the Canadian contribution to the 30 m resolution 2010/2015 LC map of North America to the joint collaborative effort by the Mexican, American, and Canadian government institutions under the

https://doi.org/10.5194/egusphere-2022-923
Preprint. Discussion started: 4 October 2022

NALCMS umbrella. The NALCMS LC map has 19 classes based on the United Nations Land Cover Classification System (LCCS; Di Gregorio, 2005). Assessment based on reference samples showed an overall accuracy of 76.6% for the year 2010 data (Latifovic et al., 2017), which is used in this study.

VLCE is an automated framework to enable annual LC mapping using time series of Landsat surface reflectance, informed by spatially explicit forest change and a *priori* knowledge of ecological succession. Temporally consistent annual LC maps representative of Canada's forested ecosystems from 1984 to 2012 were generated using the VLCE framework, characterizing LC dynamics following wildfire and harvesting events by Hermosilla et al. (2018). The VLCE maps have 12 LC classes in a hierarchical classification structure following that of the National Forest Inventory. Assessment based on reference samples showed an overall accuracy of 70.3% for the map of 2005 (the year with the greatest number of reference samples; Hermosilla et al., 2018). Land cover data from the year 2010 are used in this study.

Overall, the 19-class NALCMS product presents a more detailed LC distribution than the 12-class VLCE map over Canada. For example, areas classified as "Exposed/Barren lands" in the VLCE map correspond to either "Sub-polar or polar grassland-lichen-moss", "Sub-polar or polar barren-lichen-moss", or "Barren lands" in the NALCMS map. Areas of cropland are not separated from grassland in the VLCE map. A recent study showed that the wetland class in NALCMS suffers from large uncertainty in forest cover mapping because treed-wetland was not separated from herbaceous wetland in its legend (Wang et al., 2019). To take advantage of both datasets, we created a hybrid product by combining them through the following steps: (1) Reproject the VLCE data from its Lambert Conformal Conic projection to the same Lambert Azimuthal Equal Area projection that is used for the NALCMS data; (2) Replace pixels

https://doi.org/10.5194/egusphere-2022-923
Preprint. Discussion started: 4 October 2022

classified as “Exposed/Barren lands” and “Bryoids” in the VLCE data with the more specific LC classes from the NALCMS data; (3) Replace pixels classified as “Herbs” in the VLCE data with the “Cropland” class in the NALCMS data; (4) and merge the rest of LC classes from NALCMS to the corresponding classes in the VLCE data. There are a total of 17 classes in this new hybrid product, which we will henceforth refer to it as the Hybrid LC dataset and is shown in Figure 1.

2.2 The global LC products

The GLC2000 dataset was generated from SPOT/VEG data collected from November 1999 to December 2000 at 1 km resolution (Bartholomé and Belward, 2005). It was produced by 21 separate regional expert groups using an unsupervised image classification method. Based on the LCCS, the regional products were merged into one global product with a generalized LCCS legend of 22 classes. Assessment based on a random sampling of reference sites globally estimated an overall accuracy of 68.6% for the GLC2000 product (Mayaux et al., 2006).

The annual ESA-CCI LC data at 300 m resolution are available for the period 1992-2018, which were generated from baseline data and annual LC changes (ESA, 2017). The baseline data were generated using a combination of machine learning and unsupervised image classification methods from the entire archive of ENVISAT/ Medium Resolution Imaging Spectrometer for the period of 2003-2012. The annual LC changes were detected at 1 km resolution from the Advanced Very High Resolution Radiometer time series between 1992 and 1999, SPOT/VEG time series between 1999 and 2013, and the PROBA-V time series between 2013 and 2018. Based on the LCCS legend, the ESA-CCI LC data have 22 level 1 classes, and 15 level 2 sub-classes. Assessment based on the GlobCover validation database estimated an overall accuracy of 71% for the ESA-CCI LC product (ESA, 2017).

https://doi.org/10.5194/egusphere-2022-923
Preprint. Discussion started: 4 October 2022

2.3 Other datasets

Airborne Lidar has been used to monitor forests since the 1980s and is well suited to estimate vegetation height, volume, and biomass (Hopkinson et al., 2006; Wulder et al., 2008). Vegetation cover percentage for canopy height above 2 m from airborne Lidar data are used to estimate the fraction of tall versus low vegetation for LC classes with a mix of woody and herbaceous vegetation in this study. The Lidar data were collected along 34 survey flights across the boreal forest of Canada in the summer of 2010 by the Canadian Forest Service (Wulder et al., 2012). A 25 by 25 m tessellation was generated with the approximately 400 m wide Lidar swath, with each cell treated as an individual Lidar plot.

A tree cover fraction (TCF) dataset for 2010 is also used in this study (Hansen et al., 2013; hereafter the Hansen TCF dataset). It was based on Landsat images at 30 m resolution. In contrast to the discrete LC classification datasets (providing a certain number of LC classes) as described above, the Hansen dataset is a vegetation continuous field product (providing tree cover fractions from 0 – 100%), in which the satellite spectral information was used to estimate the TCF in each pixel using a regression tree algorithm (Hansen et al., 2002; 2010). This may better represent heterogeneous areas than is possible by discrete LC classification. Tree cover is defined to exist over pixels where canopy closure is observed for vegetation taller than 5 m in height. Forests are generally defined as woody vegetation taller than 3 m in the regional and global LC datasets. The different definitions of tree heights should not result in much difference in areas with mature forests, such as most boreal forests in Canada.

Simulated surface albedo by the CLASSIC model in offline experiments is evaluated against the Moderate Resolution Imaging Spectroradiometer (MODIS) (MCD43C3) broadband (0.3–5.0

https://doi.org/10.5194/egusphere-2022-923
Preprint. Discussion started: 4 October 2022

μm) white-sky albedo (Schaaf et al., 2002), with quality flags of 0–2 (75% or more full inversions and 25% or fewer fill values) and solar zenith angles less than 70°. The MODIS albedo product used in this study is at 0.05 degree resolution, and is regridded to the 0.22 degree model grid (see Section 2.4.2).

2.4 The CLASSIC model and simulation setup

2.4.1 The CLASSIC model

CLASSIC is the successor to the coupled modelling framework based on the Canadian Land Surface Scheme (CLASS; Verseghy, 1991; 1993) and the Canadian Terrestrial Ecosystem Model (CTEM; Arora and Boer, 2005; Melton and Arora, 2016). The physics and biogeochemistry components of CLASSIC are based on CLASS and CTEM, respectively.

For the physics component, vegetation is represented in terms of the fractional coverage of the four PFTs (needleleaf trees, broadleaf trees, crops, and grasses). The physics component represents a single snow layer with variable depth and a single vegetation canopy layer. As a first-order treatment of subgrid-scale heterogeneity, each grid cell is divided up into four sub-areas, consisting of vegetated and bare soil areas, each with and without snow cover. The grid cell albedo is computed as a weighted mean using the fractional coverages for each surface type. Canopy snow processes such as interception/unloading, sublimation, and melt are simulated by the physics module of CLASSIC. Twenty ground layers represent the soil profile, starting with 10 layers of 0.1 m thickness. The thicknesses of the layers gradually increase to 30 m for a total ground depth of over 61 m. Liquid and frozen soil moisture contents, and soil temperature, are determined prognostically for permeable soil layers.

The biogeochemistry component of CLASSIC represents vegetation in terms of nine PFTs: Needleleaf Evergreen trees (NLE), Needleleaf Deciduous trees (NLD), Broadleaf Evergreen

https://doi.org/10.5194/egusphere-2022-923
Preprint. Discussion started: 4 October 2022

trees (BLE), Broadleaf Cold Deciduous trees (BCD), Broadleaf Dry Deciduous trees (BDD), C_3 and C_4 Crops (C3C/C4C), and C_3 and C_4 Grasses (C3G/C4G). These nine PFTs map directly onto the four PFTs used by CLASSIC's physics component. When the physics and biogeochemistry components are coupled together, the structural attributes of vegetation including leaf area index, canopy mass, rooting depth, and vegetation height are simulated dynamically as a function of environmental conditions by the biogeochemistry component. When the biogeochemistry component is turned off, specified structural attributes of vegetation for use by the physics component are extracted from look-up tables.

2.4.2 Simulation set up

Gridded meteorological data based on the Climatic Research Unit (CRU, https://crudata.uea.ac.uk/cru/data/hrg/) and Japanese reanalysis (JRA) (CRUJRA) are used to drive CLASSIC simulations. The data are constructed by regridding data from the JRA and adjusting where possible to align with the CRU TS 4.05 data. The blended product from year January 1901 to December 2020 has the 6-hourly temporal resolution of a reanalysis product but monthly means adjusted to match the CRU data (Harris, 2020). The 6-hourly data are disaggregated into half-hourly data for the following seven meteorological variables that are used to force the model: 2 m air temperature, total precipitation, specific humidity, downward solar radiation flux, downward longwave radiation flux, surface pressure, and wind speed. In CLASSIC, the phase of precipitation is determined by a threshold surface air temperature with three options available (Bartlett et al., 2006). The 0°C air temperature threshold is used to partition precipitation into rain or snow in this study. This choice should not have a significant impact on the simulated surface albedo in CLASSIC (Wang et al. 2014).

https://doi.org/10.5194/egusphere-2022-923
Preprint. Discussion started: 4 October 2022

Two simulations over the 1850-2020 historical period are performed using PFTs derived from the ESA-CCI and the GLC2000 datasets respectively, which is the only difference between the two simulations. Besides land cover and meteorological forcings, CLASSIC requires globally averaged atmospheric CO_2 concentration, and geographically varying time-invariant soil texture and soil permeable depth. The atmospheric CO_2 concentration values are provided by the Global Carbon Project protocol (https://www.globalcarbonproject.org/index.htm). The soil texture information consists of the percentage of sand, clay, and organic matter and is derived from the SoilGrids250m dataset (Hengl et al., 2017), and permeable soil depth is based on Shangguan et al. (2017). The simulations are performed at a 0.22 degree rotated latitude-longitude grid over a domain including Canada and part of Alaska (Fig. 3). Pre-industrial simulations that correspond to the year 1850 are required prior to doing the historical simulations so that model's carbon pools, including leaf biomass which determines leaf area index, are spun up to near equilibrium for each land cover. The pre-industrial simulations use 1901-1920 meteorological data repeatedly with atmospheric CO_2 concentration specified at its 1850 level. Each historical simulation is then initialized from its corresponding pre-industrial simulation after it has reached equilibrium. For the period 1851-1900, the CRUJRA meteorological data for the first 20 years (1901-1920) are used repeatedly. For the 1901-2020 period the meteorological data corresponding to each actual year are used. The period from 2001 to 2015 was selected for analyzing the simulated results.

3. PFT mapping methods and results

A CW-table for the Hybrid LC map based on the Lidar plots, tree species, field surveys, and high-resolution images is first created. We then compute the sub-pixel fractional composition of the LC classes in the 300 m ESA-CCI data using the 30 m Hansen TCF and the 30 m Hybrid LC data respectively, which are in turn used to create the CW-table for the ESA-CCI dataset (Fig. 2).

https://doi.org/10.5194/egusphere-2022-923
Preprint. Discussion started: 4 October 2022

Finally the CW-table developed for the ESA-CCI dataset over Canada is extended to the whole globe as explained in Section 3.3.

3.1 CW-table for mapping Hybrid LC classes to CLASSIC PFTs

Among the nine CLASSIC PFTs, BLE and BDD forests are not present in Canada. These are primarily tropical PFTs as represented in CLASSIC. NLD only accounts for less than 1% of coniferous forests in Canada (Wang et al., 2019). Therefore we do not consider NLD, BLE, and BDD from here on in this study. Considering the fine resolution (30 m) of the Hybrid map, especially relative to the model resolution (~16 km) used in this study, we assign fractions of 1.0 to the two pure forest classes (LC210 and LC220), the cropland (LC15), and the five non-vegetative classes (LC16 to LC32) in its CW-table (Table 1). The mixed-wood category (LC230) is split evenly into NLE and BCD in the table based on the definition in the VLCE legend (Hermosilla et al., 2018; Wulder et al., 2003). Note that in Table 1, BDD and BCD, and C_3 and C_4 crops and grasses, are considered together. The reason for this is that the separation of broadleaf trees into their cold and deciduous phenotypes is based on latitude (Wang et al., 2006). The separation of crops and grasses based on their photosynthetic pathway (C_3 or C_4) is done based on the C_4 fraction from Still et al. (2003).

CLASSIC does not yet explicitly represent shrub PFTs (research on including shrubs as a separate PFT is ongoing), and therefore the fraction of tall shrubs is assigned to one of the tree PFTs as was done in creating the CW-table for GLC2000 for use with CLASSIC (Wang et al., 2006). Four (LC2, LC50, and LC80-81) out of the 17 classes in the Hybrid map are characterized by a mosaic of trees, shrubs, and herbaceous vegetation. The vegetation coverage for canopy height above 2 m from Lidar plots is used to inform the partitioning of forest (tall vegetation) to

https://doi.org/10.5194/egusphere-2022-923
Preprint. Discussion started: 4 October 2022

non-forest (low vegetation) fractions for these classes. The distribution of tree species from Beaudoin et al. (2014) is used to guide the splitting of coniferous versus broadleaf forest fractions. For example, for the Wetland-treed category (LC81), maps of tree species show that coniferous forests dominate wetland-treed regions, while broadleaf forests are generally non-existent. We, therefore, assign most of the forest fraction to NLE (0.55), only 0.05 to BCD, 0.35 to grasses, and the remaining to the bare ground for LC81 (Table 1). The presence of evergreen shrubs is rare in Canada according to National Forest Inventory ground plots data (Gillis et al., 2005), thus we only assign an estimated tall shrub fraction (0.20) in the shrub class (LC50) to BCD. The sub-polar or polar classes (LC11 to LC13) are located above the treeline and mainly consist of low shrubs and grass. The fractions of grass (including low shrubs) and bare ground are based on field surveys of fractional vegetation cover and tundra PFTs data in Bjorkman et al. (2018) and Macander et al. (2020). High-resolution images from Google Earth engine or Bing Maps are also used to examine the ratio of vegetated versus bare ground for all classes in which bare ground is present.

3.2. CW-table for mapping ESA-CCI LC classes to CLASSIC PFTs over Canada

3.2.1 The error and sub-pixel fractional error matrices

A standard approach for the accuracy assessment of LC products is to use an error matrix. It is a square array or table of numbers arranged in rows and columns, in which the classification from the LC product (usually represented by the rows) is compared to the reference data (usually represented by the columns) for each category (Congalton, 1991). The major diagonal of the matrix presents the number of correct classifications indicating the agreement between the LC and the reference data for each category. In practice, fine-resolution regional maps are often used to assess large-scale LC products derived from coarse-resolution data (Cihlar et al., 2003). In

https://doi.org/10.5194/egusphere-2022-923
Preprint. Discussion started: 4 October 2022

such cases, the fine-resolution reference data are aggregated/regridded to match the grid of the coarse-resolution data. Several classes in the reference data may be present in a single coarse-resolution pixel depending on the homogeneity of the landscape. In order to compare the reference and the LC data on a one-to-one basis, the dominant LC class (the class with the most abundant fractions based on all fine-resolution pixels in the reference data) is often assigned to the regridded reference pixel.

The sub-pixel fractional error matrices have been introduced as a more appropriate way of assessing the accuracy of mixed pixels by Latifovic and Olthof (2004). In contrast with an error matrix where only the dominant LC class is used as described above, the sub-pixel fractional error matrix is produced by assigning sub-dominant LC classes from all fine-resolution pixels in the reference data to the corresponding single coarse-resolution pixel. It thus allows a quantitative assessment of the fractional composition of the LC classes in the coarse resolution dataset. In this study, both the 30 m Hansen TCF data and the 30 m Hybrid LC map are used to compute the sub-pixel fractional error matrices of the 300 m ESA-CCI dataset (Table 2 and Table 3). However, the objective here is not an accuracy assessment as in Latifovic and Olthof (2004) but rather to obtain the fractional composition of the LC classes in the ESA-CCI product and to inform the PFT mapping process. We refer this process as the sub-pixel fractional composition analyses in the rest of this paper. Sub-pixel fractional composition analyses is first performed for each ecozone and then weighted mean fractions for each ESA-CCI cslass are computed based on pixel counts in each of the ecozones (see the location of ecozones in Fig. 1). For the Hansen TCF data, results are shown only for the ESA-CCI LC classes containing forests in Canada (Table 2). In the ESA-CCI legend (Table 4), two sub-classes for broadleaf (LC61 and LC62) and needleleaf (LC71 and LC72) forests are included as the closed (>40% forest cover)

https://doi.org/10.5194/egusphere-2022-923
Preprint. Discussion started: 4 October 2022

and open (10-40% forest cover) categories apart from the main classes (LC60 and LC70). As expected, the TCF is larger for the closed classes than for the main and the open classes (Table 2). In Table 2, we also include ratios of TCF between the main class and the closed class, and between the open class and the closed class. We note that the ratios are different for broadleaf (main class vs. closed class: 68.5/86.7=0.8; open class vs. closed class: 0.43/86.7=0.43) and needleleaf (main class vs. closed class: 39.3/61.7=0.6; open class vs. closed class: 23.2/61.7=0.38) forests, which need to be taken into account when creating the CW-table for the ESA-CCI dataset.

To obtain representative class compositions of the ESA-CCI dataset, only homogenous ESA-CCI pixels are included in the sub-pixel composition analyses based on the Hybrid LC data. The homogenous pixels are defined following the method in Herold et al. (2008). To quantify landscape heterogeneity, 3×3 pixel neighborhoods are assessed for the ESA-CCI data. A neighborhood is considered homogenous if only one LC class is present. The weighted mean fraction for each class is computed from ecozones with more than 10 homogenous ESA-CCI pixels for that class (Table 3). Only 13 out of the 37 ESA-CCI classes are included in Table 3, the rest of the classes either have limited presence in Canada or are non-vegetative (Table 4).

In the Hybrid CW-table (Table 1), four LC classes (2, 81, 210, and 230) contribute to the fractional cover of NLE, and five LC classes (50, 80, 81, 220, and 230) contribute to the fractional cover of BCD. In Table 3, we also include an integrated fractional cover (F) for NLE and BCD (last two rows) for each of the ESA-CCI classes based on the following formula:

$$F = \sum_{i=1}^{N} F1_i * F2_i \quad (1)$$

https://doi.org/10.5194/egusphere-2022-923
Preprint. Discussion started: 4 October 2022

Where $F1_i$ are fractions in Table 3, $F2_i$ are fractions in Table 1, and N is the number of Hybrid LC classes contributing to NLE (N = 4) or BCD (N = 5) as shown in Table 1. As an example, the fraction of NLE for the LC70 (Tree cover needleleaf evergreen closed to open) in ESA-CCI data in Table 3 (see the NLE row and the column for class 70) is obtained as follows: F = 0.02×0.20 + 0.17×0.55 + 0.29×1.0 + 0.09×0.5 = 0.44. This process reduces the subjectivity in assigning the ESA-CCI land cover classes to CLASSIC's two tree PFTs (NLE and BCD) that are present in Canada since the process is based on the high-resolution Hybrid LC data.

3.2.2 CW-table for the ESA-CCI LC dataset over Canada

Table 2 and Table 3 thus form the basis for creating the CW-table for mapping the ESA-CCI LC classes to CLASSIC's PFTs (Fig. 2 and Table 4). For the ESA-CCI class LC61 (Tree cover broadleaved deciduous closed) (not included in Table 3 due to limited presence in Canada), ratios of TCF for LC60 vs LC61 in Table 2 and the fractions of LC60 (Tree cover broadleaved deciduous closed to open) in Table 3 are used to derive fractions for LC61 in Table 4. The remapping of LC62 (Tree cover broadleaved deciduous open) and LC72 (Tree cover needleleaf evergreen open) into CLASSIC's PFTs is done in a similar way. Since NLD is not included in either Table 2 or Table 3, the needleleaf deciduous tree cover classes (LC80-82) are assigned to the same fractions as the needleleaf evergreen tree cover classes (LC70-72). For simplicity, the fractions in Table 3 are rounded to values with either "0" or "5" at the hundredth place when used in Table 4. For the rest of the classes not included in either Table 2 or Table 3, values are based on the default CW-table from the ESA-CCI user guide (Table 7-2, ESA, 2017). The spatial distribution of LC classes is also taken into consideration when determining the fractions in the CW-table. For example, the sparse vegetation class (LC150) is mainly distributed above the

https://doi.org/10.5194/egusphere-2022-923
Preprint. Discussion started: 4 October 2022

359 treeline in alpine and Arctic tundra environments, thus we only assign 0.05 to BCD, the rest to
360 C3G/C4G and bare ground (Table 4).

361 The six CLASSIC PFTs (those present in Canada) are produced from the Hybrid and the ESA-
362 CCI maps based on Table 1 and Table 4 respectively. The PFTs from the Hybrid map are used as
363 a reference here to map ESA-CCI land cover classes to CLASSIC's PFTs. To make the spatial
364 distribution of PFTs from ESA-CCI agree better with those from the Hybrid dataset, fractions for
365 the following classes in Table 4 are adjusted upward by 0.05: LC60 from 0.65 to 0.70 for BCD;
366 LC71 and LC81 from 0.80 to 0.85 for NLE; and LC120 from 0.10 to 0.15 for BCD. Values for
367 LC10-20 are also slightly adjusted to reduce crop fractions.

368 **3.3. CW-table for the ESA-CCI LC dataset over the globe**

369 Based on Table 4, the fractional coverage of nine CLASSIC PFTs are also produced on a global
370 scale. However, fractions of NLE in Eurasia are found to be too low relative to the Hansen TCF
371 data, with maximum values only around 0.45 in most NLE dominated areas, where the
372 maximum TCF from the Hansen dataset is around 0.80. Needleleaf evergreen forests are
373 represented by LC classes 70 (closed to open), 71 (closed), and 72 (open). Examining the ESA-
374 CCI LC map shows that in Eurasia nearly all needleleaf evergreen forests are classified as LC70
375 (closed-to-open), with only less than 400 pixels as LC71 (closed), and none as LC72 (open). In
376 contrast, in Canada 36% of needleleaf evergreen forest is classified as LC70 (closed-to-open),
377 64% as LC71 (closed), and less than 1% as LC72 (open). Sub-pixel fractional composition
378 analyses of the ESA-CCI classes based on the Hansen TCF dataset show that in Eurasia TCF for
379 LC70 (closed-to-open) is 66% and for LC71 (closed) is 35% (note few pixels with this class).
380 This is in contrast with those in Canada where TCF for LC70 (closed-to-open) is 39% and for

https://doi.org/10.5194/egusphere-2022-923
Preprint. Discussion started: 4 October 2022

LC71 (closed) is 62%, explaining the too low NLE fractions in Eurasia when mapping PFTs based on Table 4, and also the too high TCF in northwestern Canada when mapping PFTs based on the default CW-table (Wang et al., 2018). In order to apply Table 4 globally, the original LC70 (closed-to-open) was split into two classes: LC73 (a new class) which is the same as LC70 over Canada (and zero everywhere else), and LC70 (revised) which is the same as before except zero over Canada. The fractions for the new LC70 class are made the same as for LC71 in Table 4, which applies to NLE outside of Canada. Essentially, the closed-to-open needleleaf forest LC70 class over Eurasia is treated as the closed needleleaf forest.

The global PFTs based on Table 4 are used in offline CLASSIC simulations in Arora et al. (2022), who carry out a comprehensive assessment of the impact of using two different LC datasets (ESA-CCI versus GLC2000) for representing the nine CLASSIC PFTs. They also assess the effect of using land cover reconstructions based on the ESA-CCI and GLC2000 datasets on the simulated surface energy, water, and CO_2 fluxes in the CLASSIC model.

3.4 Comparison of PFTs from Hybrid, ESA-CCI, and GLC2000 data

Figure 3 shows the spatial distribution of PFTs derived from the Hybrid, ESA-CCI, and GLC2000 LC datasets respectively. C_4 crops (C4C) and grasses (C4G) are sparse in Canada as would be expected since C4 PFTs grow only in warmer temperatures when the average monthly temperature exceeds 22 °C (Fox et al., 2018). Therefore, only four out of the six PFTs (those present in Canada) are shown in Figure 3. In general, the spatial distributions of the PFTs from the ESA-CCI and the Hybrid datasets agree well except for C_3 grasses (C3G) (Fig. 3j and Fig. 3k). This is not surprising given that the CW-table for the ESA-CCI dataset is based on the Hybrid map. Areas mapped as C3G in Hybrid (Fig. 3j), were mainly classified as sparse

https://doi.org/10.5194/egusphere-2022-923
Preprint. Discussion started: 4 October 2022

vegetation (LC150) in the ESA-CCI legend (Table 4). However, LC150 from ESA-CCI was also found in some areas of the high Arctic islands, where barren land is the dominant class in the Hybrid map (grey coloured areas in Fig. 1). If too much grass were assigned to LC150, it would yield unrealistically large fractional coverage of grass in the high Arctic islands. In Table 4, for LC150, 0.05 is assigned to BCD, 0.35 to grasses, and the rest to the bare ground for LC150, which yields a total vegetation cover of 40% and is more than the definition (<15% vegetation) used in the ESA-CCI legend. Yet, this still results in less C3G and less bare ground in the ESA-CCI map (Fig. 3k and Fig. 3n) than those from the Hybrid map (Fig. 3j and Fig. 3m). This suggests that it is not ideal to classify areas in the high Arctic islands and in the Arctic tundra region as being in the same land cover category.

There are large differences in the spatial distribution of the PFTs based on the GLC2000 LC product and those based on the Hybrid and ESA-CCI datasets (Fig. 3 and Fig. 4). Relative to PFTs from ESA-CCI, GLC2000 has less NLE and more BCD in northwestern Canada, and more NLE in southern and eastern Canada (Fig. 4a and Fig. 4b). GLC2000 based CLASSIC PFT fractions also exhibit more crops, less grass, and more bare ground (Fig. 4c-4e). These differences partly stem from the differences in the ESA-CCI and GLC2000 LC datasets, but are also due to the fact how the fractions in the CW-tables of the two datasets are used to translate LC data to fractional coverage of PFTs as demonstrated in Wang et al. (2019).

3.5 Bias in simulated surface albedo and LAI

The top row of Figure 5 shows the bias in winter albedo (March) simulated by CLASSIC when using PFT distributions based on the ESA-CCI (Fig. 5a) and GLC2000 products (Fig. 5b). While model biases are the result of both the driving geophysical and meteorological data that are used

https://doi.org/10.5194/egusphere-2022-923
Preprint. Discussion started: 4 October 2022

to force the model, as well as the model itself, the comparison between the two simulations does show the effect of differences in the distribution of PFTs. Relative to observed surface albedo from MODIS, there are relatively large negative biases in the southwest of Hudson Bay and central Quebec, while there are relatively large positive biases in western Canada and Alaska in the simulation when using the GLC2000 product to obtain PFT distributions (Fig. 5b). Both the negative and the positive biases are largely reduced in the simulation using PFT distributions based on the ESA-CCI product (Fig. 5a). The lower row of Figure 5 shows the spatial distribution of the difference in surface albedo (Fig. 5c) and leaf area index (Fig. 5d) between the two simulations, which are closely correlated (r = -0.85). Given the same meteorological forcing dataset is used to drive both simulations, the differences in the simulated LAI are due mainly to the different PFT distributions used in the two simulations. Since NLE is the only PFT with LAI > 0 during winter in Canada, the LAI difference in March as shown in Figure 5d is mainly due to the different fractional coverage of NLE based on the ESA-CCI and GLC2000 products (Fig. 4a).

In contrast, the large positive albedo biases (up to ~ 0.4) in southern Canada are more or less the same in both simulations (Fig. 5a and Fig. 5b), where the dominant PFT is C3 crops (Fig. 3h and Fig. 3i). Those positive albedo biases are likely due to the standing crop stubble not treated in CLASSIC currently. Harder et al. (2018) showed that the height of the stubble over wheat and canola field in Saskatchewan, Canada may range from 10 to 40 cm, with a maximum PAI (plant area index) of 1.0. Wang et al. (2016) showed that surface albedo in CLASSIC decreased exponentially with increasing PAI for the bare or snow-covered canopy over snow, while most reductions of the albedo were achieved through the increase of PAI from 0 to 1.0. They showed that surface albedo decreased from 0.75 to 0.31 in CLASSIC when PAI increased from 0 to 1.0

https://doi.org/10.5194/egusphere-2022-923
Preprint. Discussion started: 4 October 2022

for the bare canopy over snow, which appears to fully account for the positive albedo biases in the agricultural areas of southern Canada (Fig. 5a and Fig. 5b). Improvements to the crop module of CLASSIC to improve cropland albedo are currently being considered.

4. Summary and conclusions

A hybrid land cover map at 30 m resolution is created by merging the NALCMS and VLCE land cover products over Canada. Vegetation height data from Lidar plots, tree species, and high resolution images are used to inform the creation of a CW-table for mapping the 17 LC classes of the Hybrid map to six CLASSIC PFTs that are present in Canada. Both the Hybrid map and the Hansen tree cover fraction data are used to compute the sub-pixel fractional composition of the LC classes in the ESA-CCI LC dataset, which is then used to create a cross-walking table for mapping the 37 ESA-CCI categories to CLASSIC PFTs. Based on the new CW-tables, PFT distributions are produced from the Hybrid and the ESA-CCI LC products, respectively, and are compared with those based on the GLC2000 dataset currently used in CLASSIC. The results show that the spatial distribution of PFTs from the ESA-CCI dataset is in better agreement with those from the Hybrid map, while there are large differences in the PFTs from the GLC2000 dataset and from the Hybrid/ESA-CCI datasets.

CLASSIC simulations driven with meteorological data from the CRU-JRA product show that the simulated winter albedo is improved when using PFT distributions based on the ESA-CCI LC product compared to that based on the GLC2000 product, which is consistent with findings from previous studies. While, CLASSIC simulations could also have been performed using its PFT distributions based on the Hybrid LC product, the reason for using the ESA-CCI based PFT fractions for CLASSIC is that ESA-CCI is a global product. CLASSIC simulations are routinely

https://doi.org/10.5194/egusphere-2022-923
Preprint. Discussion started: 4 October 2022

performed at the global scale both in the framework of the Canadian Earth System Model (Swart et al., 2019), where CLASSIC serves as its land component, and offline where global CLASSIC simulations driven with the CRU-JRA meteorological data contribute to the annual global carbon budget assessments of the Global Carbon Project (Friedlingstein et al., 2020). Untreated crop stubble appears to be the cause for positive winter albedo biases in southern Canada, which needs to be addressed in a future version of CLASSIC. These results underscore the importance of accurate representation of vegetation distribution in a realistic simulation of surface albedo in LSMs.

Previous methods for mapping PFTs from LC datasets are mainly based on class descriptions, expert knowledge, and the spatial distribution of global biomes, which is a largely subjective process. As a consequence, a PFT method developed for mapping one LC dataset to PFTs represented in one model can not be easily transferred to other LC datasets even for deriving PFTs in the same model. The development of satellite and computing technology has enabled the creation of more detailed global LC products at finer spatial resolutions in recent years, however, the lack of an objective PFT mapping method impedes the implementation of the new improved LC products in LSMs. Here, we have proposed a method to inform the cross-walking process using sub-pixel fractional composition analyses based on a tree cover fraction dataset and a fine-resolution LC map. Our results suggest that the sub-pixel fractional composition analyses provide an effective way to reduce uncertainties in the cross-walking process and therefore, to some extent, objectifies the otherwise subjective process. The PFT mapping approach developed in this study can also be applied to other LC datasets for mapping PFTs used in other LSMs.

https://doi.org/10.5194/egusphere-2022-923
Preprint. Discussion started: 4 October 2022

Acknowledgements.

We'd like to thank Mike Brady (ECCC) for his help with data processing and especially for creating the Hybrid map, and Mike Wulder from the Canadian Forest Service of Natural Resources Canada for providing the Lidar plots data and for helping interpret the Lidar data and the VLCE land cover map.

References

Arora, V. K., Boer, G. J.: A parameterization of leaf phenology for the terrestrial ecosystem component of climate models. Glob. Chang. Biol., 11, 39–59, 2005.

Arora, V. K. and Boer, G. J.: Uncertainties in the 20th century carbon budget associated with land use change, Glob. Change Biol., 16, 3327–3348, https://doi.org/10.1111/j.1365-2486.2010.02202.x, 2010.

Arora, V. K., Boer, G. J., Christian, J. R., Curry, C. L., Denman, K. L., Zahariev, K., Flato, G. M., Scinocca, J. F., Merryfield, W. J., and Lee, W. G.: The Effect of Terrestrial Photosynthesis Down Regulation on the Twentieth-Century Carbon Budget Simulated with the CCCma Earth System Model, J. Clim., 22, 6066–6088, https://doi.org/10.1175/2009JCLI3037.1, 2009.

Beaudoin, A., Bernier, P.Y., Guindon, L., Villemaire, P., Guo, X.J., Stinson, G., Bergeron, T., Magnussen, S., and Hall, R.J.: Mapping attributes of Canada's forests at moderate resolution through kNN and MODIS imagery, Can. J. For. Res. 44: 521–532, dx.doi.org/10.1139/cjfr-2013-0401, 2014.

https://doi.org/10.5194/egusphere-2022-923
Preprint. Discussion started: 4 October 2022

512 Bartholomé, E., and Belward, A. S.: GLC2000: A new approach to global land cover mapping
513 from Earth Observation data, Int. J. Remote Sens., 26, 1959–1977, 2005.

514 Bartlett, P. A., MacKay, M. D., and Verseghy, D. L.: Modified snow algorithms in the Canadian
515 land surface scheme: Model runs and sensitivity analysis at three boreal forest stands, Atmos.–
516 Ocean, 44, 207–222, 2006.

517 Bartlett, P. A., and Verseghy, D. L.: Modified treatment of intercepted snow improves the
518 simulated forest albedo in the Canadian land surface scheme, Hydrol. Process., 29, 3208–3226,
519 https://doi:10.1002/hyp.10431, 2015.

520 Betts, R. A.: Biogeophysical impacts of land use on present-day climate: near-surface
521 temperature change and radiative forcing, Atmos. Sci. Lett., 2, 39–51,
522 https://doi.org/10.1006/asle.2001.0037, 2001.

523 Bjorkman, A. D., Myers-Smith, I. H., Elmendorf, S.C. et al.: Plant functional trait change across
524 a warming tundra biome, Nature, 562, 57–62, https://doi.org/10.1038/s41586-018-0563-7, 2018.

525 Bonan, G. B., Levis, S., Kergoat, L., Oleson, K. W.: Landscapes as patches of plant functional
526 types: An integrating concept for climate and ecosystem models, Global Biogeochem. Cycles,
527 16(2), 1021, https://doi:10.1029/2000GB001360, 2002.

528 Bontemps, S., Herold, M., Kooistra, L., van Groenestijn, A., Hartley, A., Arino, O., Moreau, I.,
529 Defourny, P.: Revisiting land cover observation to address the needs of the climate modeling
530 community, Biogeosciences, 9, 2145–2157, https://doi:10.5194/bg-9-2145-2012, 2012.

https://doi.org/10.5194/egusphere-2022-923
Preprint. Discussion started: 4 October 2022

Di Gregorio, A.: Land Cover Classification System – Classification concepts and user manual for Software version 2, FAO Environment and Natural Resources Service Series, No. 8, Rome, 208pp, 2005.

ESA: Land Cover CCI Product User Guide Version 2. Tech. Rep., Available at: maps.elie.ucl.ac.be/CCI/viewer/download/ESACCI-LC-Ph2-PUGv2_2.0.pdf, 2017.

Fox, D.L., Pau, S., Taylor, L., Strömberg, C. A. E., Osborne, C.P., Bradshaw, C., Conn, S., Beerling, D.J., and Still, C.J.: limatic Controls on C4 Grassland Distributions During the Neogene: A Model-Data Comparison, Frontiers in Ecology and Evolution, 6, https://doi:10.3389/fevo.2018.00147, 2018.

Friedlingstein, P., O'Sullivan, M., Jones, M. W., Andrew, R. M., Hauck, J., Olsen, A., Peters, G. P., Peters, W., Pongratz, J., Sitch, S., Le Quéré, C., Canadell, J. G., Ciais, P., Jackson, R. B., Alin, S., Aragão, L. E. O. C., Arneth, A., Arora, V., Bates, N. R., Becker, M., Benoit-Cattin, A., Bittig, H. C., Bopp, L., Bultan, S., Chandra, N., Chevallier, F., Chini, L. P., Evans, W., Florentie, L., Forster, P. M., Gasser, T., Gehlen, M., Gilfillan, D., Gkritzalis, T., Gregor, L., Gruber, N., Harris, I., Hartung, K., Haverd, V., Houghton, R. A., Ilyina, T., Jain, A. K., Joetzjer, E., Kadono, K., Kato, E., Kitidis, V., Korsbakken, J. I., Landschützer, P., Lefèvre, N., Lenton, A., Lienert, S., Liu, Z., Lombardozzi, D., Marland, G., Metzl, N., Munro, D. R., Nabel, J. E. M. S., Nakaoka, S.-I., Niwa, Y., O'Brien, K., Ono, T., Palmer, P. I., Pierrot, D., Poulter, B., Resplandy, L., Robertson, E., Rödenbeck, C., Schwinger, J., Séférian, R., Skjelvan, I., Smith, A. J. P., Sutton, A. J., Tanhua, T., Tans, P. P., Tian, H., Tilbrook, B., van der Werf, G., Vuichard, N., Walker, A. P., Wanninkhof, R., Watson, A. J., Willis, D., Wiltshire, A. J., Yuan, W., Yue, X., and Zaehle, S.: Global Carbon Budget 2020, Earth Syst. Sci. Data, 12, 3269–3340, https://doi.org/10.5194/essd-12-3269-2020, 2020.

https://doi.org/10.5194/egusphere-2022-923
Preprint. Discussion started: 4 October 2022

554 Fritz, S., See, L., McCallum, I., Schill, C., Obersteiner, M., van der Velde, M., Boettcher, H.,
555 Havlík, P., Achard, F.: Highlighting continued uncertainty in global land cover maps for the user
556 community, Environ. Res. Lett., 6, 44005. https://dx.doi.org/10.1088/1748-9326/6/4/044005,
557 2011.

558 Georgievski, G., Hagemann, S.: Characterizing uncertainties in the ESA-CCI land cover map of
559 the epoch 2010 and their impacts on MPI-ESM climate simulations, Theor. Appl. Climatol., 137,
560 1587–1603, https://doi.org/10.1007/s00704-018-2675-2, 2019.

561 Gillis, M. D., Omule, A. Y., and Brierley, T.: Monitoring Canada's forests: The National Forest
562 Inventory, The Forestry Chronicle, 81(2): 214-221, https://doi.org/10.5558/tfc81214-2, 2005.

563 Harris, I. C.: CRU JRA v2.1: A forcings dataset of gridded land surface blend of Climatic
564 Research Unit (CRU) and Japanese reanalysis (JRA) data; Jan. 1901 - Dec. 2019, Centre for
565 Environmental Data Analysis, University of East Anglia Climatic Research Unit,
566 https://catalogue.ceda.ac.uk/uuid/10d2c73e5a7d46f4ada08b0a26302ef7, 2020

567 Hartley, A. J., MacBean, N., Georgievski, G., Bontemps, S.: Uncertainty in plant functional type
568 distributions and its impact on land surface models, Remote Sens. Environ., 203, 71–89,
569 https://doi.org/10.1016/j.rse.2017.07.037, 2017.

570 Harder, P., Warren D. H., and Pomeroy, J. W.: Modeling the Snowpack Energy Balance during
571 Melt under Exposed Crop Stubble, J. Hydrometeorol., 19, 1191-1214, https://DOI:
572 10.1175/JHM-D-18-0039.1, 2018.

https://doi.org/10.5194/egusphere-2022-923
Preprint. Discussion started: 4 October 2022

573 Hansen, M. C., DeFries, R. S., Townshend, J. R. G., Sohlberg, R., Dimiceli, C., Carroll, M. L.:
574 Towards an operational MODIS continuous field of percent tree cover algorithm: Examples us-
575 ing AVHRR and MODIS data, Remote Sens. Environ., 83, 303–319, 2002.

576 Hansen, M. C., Stehman, S. V., Potapov, P. V.: Quantification of global gross forest cover loss,
577 P. Natl. Acad. Sci., 107, 8650–8655, https://doi.org/10.1073/pnas.0912668107, 2010.

578 Hansen, M. C., Potapov, P. V., Moore, R., Hancher, M., Turubanova, S. A., Tyukavina, A.,
579 Thau, D., Stehman, S. V., Goetz, S. J., Loveland, T.R., et al.: Highresolution global maps of
580 21st-century forest cover change, Science, 342, 850–853, https://DOI: 10.1126/science.1244693,
581 2013.

582 Hengl, T., Mendes de Jesus, J., Heuvelink, G. B. M., Ruiperez Gonzalez, M., Kilibarda, M.,
583 Blagotić, A., Shangguan, W., Wright, M. N., Geng, X., Bauer-Marschallinger, B., Guevara, M.
584 A., Vargas, R., MacMillan, R. A., Batjes, N. H., Leenaars, J. G. B., Ribeiro, E., Wheeler, I.,
585 Mantel, S., and Kempen, B.: SoilGrids250m: Global gridded soil information based on machine
586 learning, PLOS ONE, 12, 1–40, https://doi.org/10.1371/journal.pone.0169748, 2017

587 Hermosilla, T., Wulder, M. A., White, J. C., Coops, N. C., Hobart, G.W.: Disturbance informed
588 annual land cover classification maps of Canada's forested ecosystems for a 29-year Landsat
589 time series. Can. J. Remote. Sens., 44, 67–87. https://doi.org/10.1080/07038992.2018.1437719,
590 2018.

591 Herold, M., Mayaux, P., Woodcock, C. E., BaESACCIni, A., Schmullius, C.: Some Challenges
592 in Global Land Cover Mapping: An Assessment of Agreement and Accuracy in Existing 1 km
593 Datasets, Remote Sens. Environ., 112, 2538–2556, 2008.

https://doi.org/10.5194/egusphere-2022-923
Preprint. Discussion started: 4 October 2022

Hopkinson, C., Chasmer, L., Lim, K., Treitz, P., and Creed, I.: Towards a universal lidar canopy height indicator, Canadian Journal of Remote Sensing, 32 (2), 139-152, https://doi: 10.5589/m06-006, 2006.

Latifovic, R., Pouliot, D., and Olthof, I.: Circa 2010 Land Cover of Canada: Local Optimization Methodology and Product Development, Remote Sens., 9, 1098, https://doi.org/10.3390/rs9111098, 2017.

Latifovic, R., and Olthof, I.: Accuracy assessment using sub-pixel fractional error matrices of global land cover products derived from satellite data, Remote Sens. Environ., 90, 153–165, 2004.

Macander, M. J., Frost, G. V., Nelson, P. R., and Swingley, C. S.: ABoVE: Tundra Plant Functional Type Continuous-Cover, North Slope, Alaska, 2010-2015, ORNL DAAC, Oak Ridge, Tennessee, USA, https://doi.org/10.3334/ORNLDAAC/1830, 2020.

Mayaux, P., Eva, H., Gallego, J., Strahler, A. H., Herold, M., Agrawal, S., Naumov, S., De Miranda, E. E., Di Bella, C. M., Ordoyne, C., et al.: Validation of the Global Land Cover 2000 Map. IEEE Trans. Geosci. Remote Sens., 44, 1728–1739, 2006.

Melton, J. R. and Arora, V. K.: Competition between plant functional types in the Canadian Terrestrial Ecosystem Model (CTEM) v. 2.0, Geosci Model Dev, 9, 323–361, https://doi.org/10.5194/gmd-9-323-2016, 2016.

Melton, J. R., Arora, V. K., Wisernig-Cojoc, E., Seiler, C., Fortier, M., Chan, E., and Teckentrup, L.: CLASSIC v1.0: the open-source community successor to the Canadian Land Surface Scheme (CLASS) and the Canadian Terrestrial Ecosystem Model (CTEM) – Part 1:

https://doi.org/10.5194/egusphere-2022-923
Preprint. Discussion started: 4 October 2022

615 Model framework and site-level performance, Geosci. Model Dev. Discuss., 1–40,
616 https://doi.org/10.5194/gmd-2019-329, 2019.

617 Moody, E. G., King, M. D., Schaaf, C. B., Hall, D. K., Platnick, S.: Northern Hemisphere five-
618 year average (2000–2004) spectral albedos of surfaces in the presence of snow: statistics
619 computed from Terra MODIS land products, Remote Sens. Environ., 111, 337–345, https://DOI:
620 10.1016/j.rse.2007.03.026, 2007.

621 Ottlé, C., Lescure, J., Maignan, F., Poulter, B., Wang, T., and Delbart, N.: Use of various remote
622 sensing land cover products for plant functional type mapping over Siberia, Earth Syst. Sci. Data,
623 5, 331–348, https://doi:10.5194/essd-5-331-2013, 2013.

624 Pielke, R. A., Avissar, R., Raupach, M., Dolman, A. J., Zeng, X., Denning, S.: Interactions
625 between the atmosphere and terrestrial ecosystem: influence on weather and climate, Global
626 Change Biol., 4, 461–475, 1998.

627 Poulter, B., Ciais, P., Hodson, E., Lischke, H., Maignan, F., Plummer, S., and Zimmermann, N.
628 E.: Plant functional type mapping for earth system models, Geosci. Model Dev., 4, 993–1010,
629 https://doi.org/10.5194/gmd-4-993-2011, 2011.

630 Poulter, B., MacBean, N., Hartley, A., Khlystova, I., Arino, O., Betts, R., Bontemps, S.,
631 Boettcher, M., Brockmann, C., Defourny, P., Hagemann, S., Herold, M., Kirches, G., Lamarche,
632 C., Lederer, D., Ottlé, C., Peters, M., and Peylin, P.: Plant functional type classification for earth
633 system models: results from the European Space Agency's Land Cover Climate Change
634 Initiative, Geosci. Model Dev., 8, 2315–2328, https://doi.org/10.5194/gmd-8-2315-2015, 2015.

https://doi.org/10.5194/egusphere-2022-923
Preprint. Discussion started: 4 October 2022

635 Schaaf, C. B., et al.: First operational BRDF, albedo nadir reflectance products from MODIS,
636 Remote Sens. Environ., 83, 135–148, https://doi:10.1016/S0034-4257(02)00091-3, 2002.

637 Shangguan, W., Hengl, T., Mendes de Jesus, J., Yuan, H., and Dai, Y.: Mapping the global depth
638 to bedrock for land surface modeling, J. Adv. Model. Earth Syst., 9, 65–88,
639 https://doi.org/10.1002/2016MS000686, 2017.

640 Smith, T. M., Shugart, H. H., and Woodward, F. I.: Plant functional types: their relevance to
641 ecosystem properties and global change, Cambridge University Press, New York, 369 pp., 1997.

642 Sterling, S. M., Ducharne, A., Polcher, J.: The impact of global land-cover change on the
643 terrestrial water cycle. Nat. Clim. Chang., 3, 385–390. http://dx.doi.org/10.1038/nclimate1690,
644 2013.

645 Still, C. J., and Berry, J. A.: Global distribution of C3 and C4 vegetation: Carbon cycle
646 implications, Global Biogeochem. Cycles, 17(1), 1006, doi:10.1029/2001GB001807, 2003.

647 Sun, W., Liang, S., Xu, G., Fang, H., and Dickinson, R. E.: Mapping plant functional types from
648 MODIS data using multisource evidential reasoning, Remote Sens. Environ., 112, 1010–1024,
649 https://doi.org/10.1016/j.rse.2007.07.022, 2008.

650 Swart, N. C., Cole, J. N. S., Kharin, V. V., Lazare, M., Scinocca, J. F., Gillett, N. P., Anstey, J.,
651 Arora, V., Christian, J. R., Hanna, S., Jiao, Y., Lee, W. G., Majaess, F., Saenko, O. A., Seiler, C.,
652 Seinen, C., Shao, A., Sigmond, M., Solheim, L., von Salzen, K., Yang, D., and Winter, B.: The
653 Canadian Earth System Model version 5 (CanESM5.0.3), Geosci. Model Dev., 12, 4823–4873,
654 https://doi.org/10.5194/gmd-12-4823-2019, 2019.

https://doi.org/10.5194/egusphere-2022-923
Preprint. Discussion started: 4 October 2022

655 Tsendbazar, N. E., de Bruin, S., Mora, B., Schouten, L., Herold, M.: Comparative assessment of
656 thematic accuracy of GLC maps for specific applications using existing reference data, Int. J.
657 Appl. Earth Obs. Geoinf., 44, 124–135, https://doi.org/10.1016/j.jag.2015.08.009, 2016.

658 Wulder, M.A., Nelson, T.: EOSD land cover classification legend report: Version 2, Natural
659 Resources Canada, Canadian Forest Service, Pacific Forestry Centre, Victoria, British Columbia,
660 Cana-da, 13 January 2003, 83pp., Available from
661 http://www.pfc.forestry.ca/eosd/cover/EOSD_Legend_Report-v2.pdf.

662 Wulder, M.A., Bater, C.W., Coops, N.C., Hilker, T., and White, J.C.: The role of LiDAR in
663 sustainable forest management, The Forestry Chronicle, 84 (6), 807- 826, 2008.

664 Wulder, M.A., White, J.C., Bater, C.W., Coops, N.C., Hopkinson, C., Chen, G.: Lidar plots - a
665 new large-area data collection option: context, concepts, and case study. Can. J. Remote. Sens.
666 38, 600–618, https://doi.org/10.5589/m12-049, 2012.

667 Verseghy, D. L.: CLASS—A Canadian Land Surface Scheme for GCMs, I. Soil model, Int. J.
668 Climatol., 11, 111–133, https://doi.org/10.1002/joc.3370110202, 1991.

669 Verseghy, D., McFarlane, N., and Lazare, M.: Class - A Canadian land surface scheme for
670 GCMs. II: Vegetation model and coupled runs, Int. J. Climatol., 13, 347–370,
671 https://doi:10.1002/joc.3370130402, 1993.

672 Wang, A., Price, D. T., Arora, V. K.: Estimating changes in global vegetation cover (1850-2100)
673 for use in climate models, Global Biogeochem. Cy., 20, https://doi:10.1029/2005GB002514,
674 2006.

https://doi.org/10.5194/egusphere-2022-923
Preprint. Discussion started: 4 October 2022

675 Wang, L., MacKay, M., Brown, R., Bartlett, P., Harvey, R., and Langlois, A.: Application of
676 satellite data for evaluating the cold climate performance of the Canadian Regional Climate
677 model over Québec, Canada, J. Hydrometeorol., 15, 614–630, https://doi.org/10.1175/JHM-D-
678 13-086.1, 2014.

679 Wang, L., Cole, J. N.S., Bartlett, P., Verseghy, D., Derksen, C., Brown, R., von Salzen, K.:
680 Investigating the spread in surface albedo for snow-covered forests in CMIP5 models, J.
681 Geophys. Res. Atmos., 121, 1104–1119, https://doi:10.1002/2015JD023824, 2016.

682 Wang, L., Bartlett, P., Chan, E., and Xiao, M.: Mapping of Plant Functional Type from Satellite-
683 Derived Land Cover Datasets for Climate Models, In Proceedings of the 2018 IEEE International
684 Geoscience and Remote Sensing Symposium, Valencia, Spain, 22–27, https://DOI:
685 10.1109/IGARSS.2018.8518046, 2018.

686 Wang, L., Bartlett, P., Pouliot, D., Chan, E., Lamarche, C., Wulder, M.A., Defourny, P., Brady,
687 M.: Comparison and Assessment of Regional and Global Land Cover Datasets for Use in
688 CLASS over Canada, Remote Sens., 11(19), 2286; https://doi.org/10.3390/rs11192286, 2019.

689
690
691
692
693
694
695
696
697

https://doi.org/10.5194/egusphere-2022-923
Preprint. Discussion started: 4 October 2022

698 Table 1. Cross-walking table for mapping the 30 m Hybrid land cover map to CLASSIC PFTs in Canada.

ID	Map description	1 NLE	2 NLD	3 BLE	4+5 BCD BDD	6+7 C3C C4C	8+9 C3G C4G	Urban	Lake	Bare
2	Sub-polar taiga needleleaf forest	0.20					0.60			0.20
11	Sub-polar or polar shrubland-lichen-moss						0.65			0.35
12	Sub-polar or polar grassland-lichen-moss						0.45			0.55
13	Sub-polar or polar barren-lichen-moss						0.10			0.90
15	Cropland					1.0				
16	Barren lands									1.0
17	Urban							1.0		
20	Water								1.0	
31	Snow_ice									1.0
32	Rock_rubble									1.0
50	Shrubland				0.20		0.60			0.20
80	Wetland				0.05		0.85			0.10
81	Wetland-treed	0.55			0.05		0.35			0.05
100	Herbs						0.80			0.20
210	Coniferous	1.0								
220	Broadleaf				1.0					
230	Mixedwood	0.50			0.50					

699

700

701

702

703

704

705

706

707

708

709

https://doi.org/10.5194/egusphere-2022-923
Preprint. Discussion started: 4 October 2022

Table 2. The sub-pixel fractional tree cover fraction for ESA-CCI LC classes (with forest cover) based on the Hansen TCF dataset in Canada. Ratios of TCF between the main class and the closed class, and between the open class and the closed class are also included.

ESA-CCI class	ESA-CCI class description	Tree cover Fraction (%)	Ratio of TCF relative to closed class
30	Mosaic cropland (>50%) / natural vegetation (<50%)	13.7	
40	Mosaic natural vegetation (>50%) / cropland (<50%)	45	
60	Tree cover broadleaved deciduous closed to open (>15%)	68.5	0.8
61	Tree cover broadleaved deciduous closed (>40%)	86.7	1
62	Tree cover broadleaved deciduous open (15-40%)	37.4	0.43
70	Tree cover needleleaf evergreen closed to open (>15%)	39.3	0.6
71	Tree cover needleleaf evergreen, closed (>40%)	61.7	1
72	Tree cover needleleaf evergreen open (15-40%)	23.2	0.38
90	Tree cover Mixed	80.9	
100	Mosaic tree and shrub (>50%) / herbaceous cover (<50%)	37.3	
110	Mosaic herbaceous cover (>50%) / tree and shrub (<50%)	19.6	
120	Shrubland	28.1	
150	Sparse vegetation (tree shrub herbaceous cover) (< 15%)	4	
160	Tree cover, flooded fresh/brackish	43	
180	Shrub or herbaceous cover, flooded	26.9	

https://doi.org/10.5194/egusphere-2022-923
Preprint. Discussion started: 4 October 2022

721 Table 3. The sub-pixel fractional composition for ESA-CCI classes (columns, homogenous ESA-CCI
722 pixels) based on the Hybrid LC map (rows) for dominant LC classes in Canada. The fractions for NLE
723 and BCD are computed based on equation (1).

Hybrid/ ESACCI Class	Hybrid description	30	40	60	70	71	90	100	120	130	140	150	160	180
2	Sub-polar taiga needleleaf forest				0.02			0.01		0.01				
11	Sub-polar/polar shrubland-lichen-moss										0.01	0.05		
12	Sub-polar/polar grassland-lichen-moss				0.04				0.03	0.01	0.24	0.27	0.03	0.04
13	Sub-polar/polar barren-lichen-moss				0.02			0.01	0.02	0.01	0.34	0.09		0.02
15	Cropland	0.92	0.37	0.02						0.1				
16	Barren lands									0.01	0.15	0.17		
50	Shrubland	0.01	0.07	0.06	0.13	0.05	0.04	0.32	0.46	0.09	0.14	0.25	0.06	
80	Wetland		0.03	0.08	0.2	0.05	0.03	0.27	0.2	0.02	0.06	0.09	0.37	0.75
81	Wetland treed		0.01	0.01	0.17	0.07	0.03	0.11	0.12				0.43	0.15
100	Herbs	0.06	0.27	0.08	0.02		0.02	0.06	0.09	0.72	0.01	0.03	0.01	0.01
210	Coniferous		0.01	0.02	0.29	0.72	0.07	0.04	0.03		0.01	0.02	0.06	
220	Broadleaf	0.01	0.13	0.57	0.02	0.01	0.28	0.07	0.01	0.01			0.01	
230	Mixedwood		0.1	0.14	0.09	0.07	0.52	0.12	0.03				0.02	
NLE	Needleleaf evergreen		0.07	0.09	0.44	0.8	0.32	0.19	0.16	0.01	0.02	0.05	0.31	0.08
BCD	Broadleaf cold deciduous	0.01	0.19	0.66	0.09	0.06	0.57	0.18	0.09	0.02	0.02	0.03	0.05	0.03

724
725
726
727
728
729
730

https://doi.org/10.5194/egusphere-2022-923
Preprint. Discussion started: 4 October 2022

731 Table 4. Cross-walking table for mapping ESA-CCI land cover dataset to CLASSIC PFTs.

ID	ESA-CCI class description	1 NLE	2 NLD	3 BLE	4+5 BCD BDD	6+7 C3C C4C	8+9 C3G C4G	Urban	Lake	Ocean	Bare
10	Cropland, rainfed (CR)					0.80	0.20				
11	CR Herbaceous cover					0.90	0.10				
12	CR Tree or shrub cover				0.60		0.30				0.10
20	Cropland, irrigated or post-flood				0.05	0.85	0.10				
30	Mosaic cropland (>50%) / natural vegetation (tree, shrub, herb)	0.05			0.15	0.60	0.20				
40	Mosaic natural vegetation (tree,shrub, herb) >50% / crop	0.10			0.20	0.40	0.30				
50	Tree cover broadleaved evergreen closed to open			0.95	0.05		0.0				
60	Tree cover broadleaved deciduous closed to open				0.70		0.25				0.05
61	Tree cover broadleaved deciduous closed				0.90		0.10				
62	Tree cover broadleaved deciduous open				0.40		0.40				0.20
70	Tree cover needleleaf evergreen closed to open	0.85			0.05		0.10				
71	Tree cover needleleaf evergreen, closed	0.85			0.05		0.10				
72	Tree cover needleleaf evergreen open	0.35			0.10		0.40				0.15
73	Replace LC70 in Canada	0.45			0.10		0.30				0.15
80	Tree cover needleleaf deciduous closed to open	0.05	0.40		0.10		0.35				0.10
81	Tree cover needleleaf deciduous closed	0.05	0.80		0.05		0.15				
82	Tree cover needleleaf deciduous open	0.05	0.30		0.10		0.45				0.15
90	Tree cover Mixed	0.25	0.05		0.60		0.10				
100	Mosaic tree and shrub (>50%) / herbaceous cover (<50%)	0.15	0.05		0.20		0.45				0.15
110	Mosaic herbaceous cover (>50%) / tree and shrub (<50%)	0.05	0.05		0.10		0.65				0.15
120	Shrubland				0.30		0.45				0.25
121	Shrubland evergreen	0.15		0.15			0.45				0.25
122	Shrubland deciduous				0.30		0.45				0.25

https://doi.org/10.5194/egusphere-2022-923
Preprint. Discussion started: 4 October 2022

130	Grassland						0.70				0.30
140	Lichens and mosses						0.20				0.80
150	Sparse vegetation (tree shrub herbaceous cover) (< 15%)				0.05		0.35				0.60
151	Sparse tree (<15%)				0.05		0.35				0.60
152	Sparse shrub (<15%)						0.30				0.70
153	Sparse herbaceous cover (<15%)						0.30				0.70
160	Tree cover, flooded fresh/brackish	0.30			0.10		0.45		0.1		0.05
170	Tree cover, flooded saline water	0.30			0.10		0.40			0.1	0.10
180	Shrub or herbaceous cover, flooded	0.10			0.05		0.45		0.15	0.15	0.10
190	Urban areas	0.025			0.025		0.15	0.75	0.05		
200	Bare areas										1.0
201	Consolidated bare areas										1.0
202	Unconsolidated bare areas										1.0
210	Water bodies								1.0		
220	Permanent snow and ice										1.0

https://doi.org/10.5194/egusphere-2022-923
Preprint. Discussion started: 4 October 2022

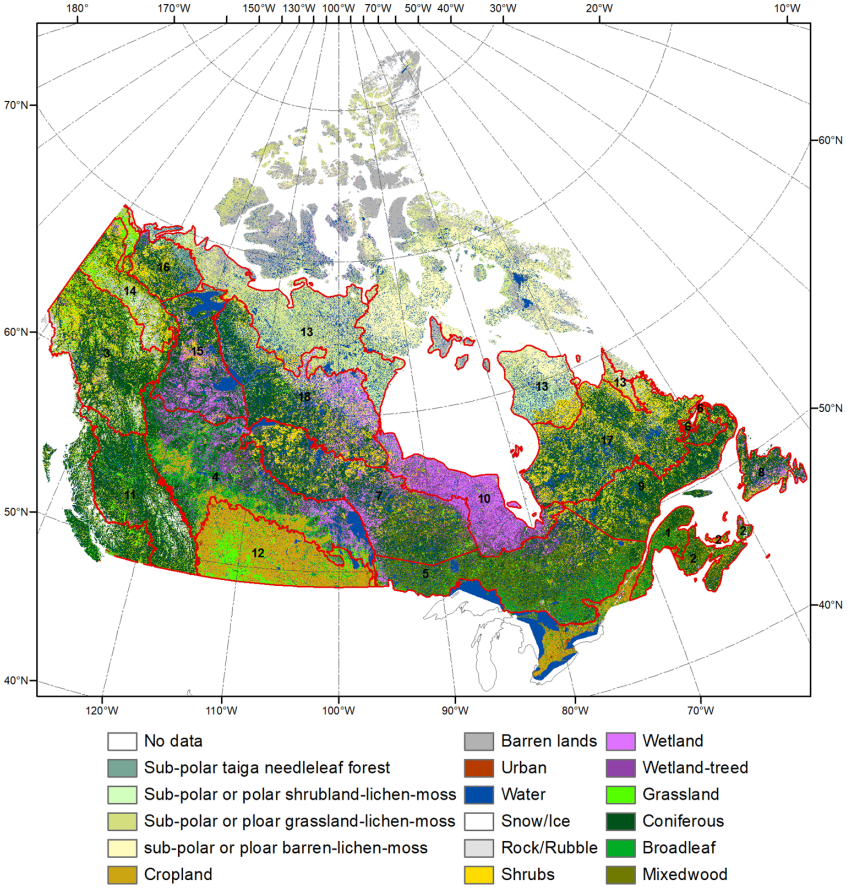

Figure 1. The Hybrid map of Canada based on VLCE and NALCMS land cover maps for 2010. The red polygons represent 18 ecozones used in this study.

https://doi.org/10.5194/egusphere-2022-923
Preprint. Discussion started: 4 October 2022

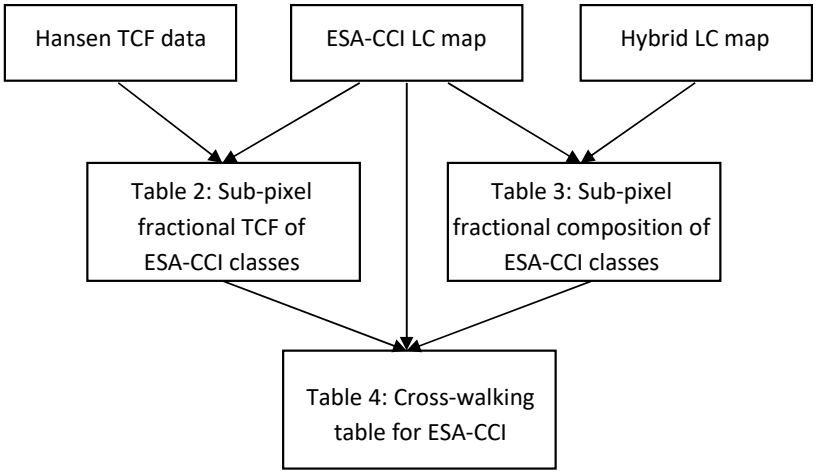

Figure 2. Schematic flow chart of the process for creating the cross-walking table for ESA-CCI LC dataset.

https://doi.org/10.5194/egusphere-2022-923
Preprint. Discussion started: 4 October 2022

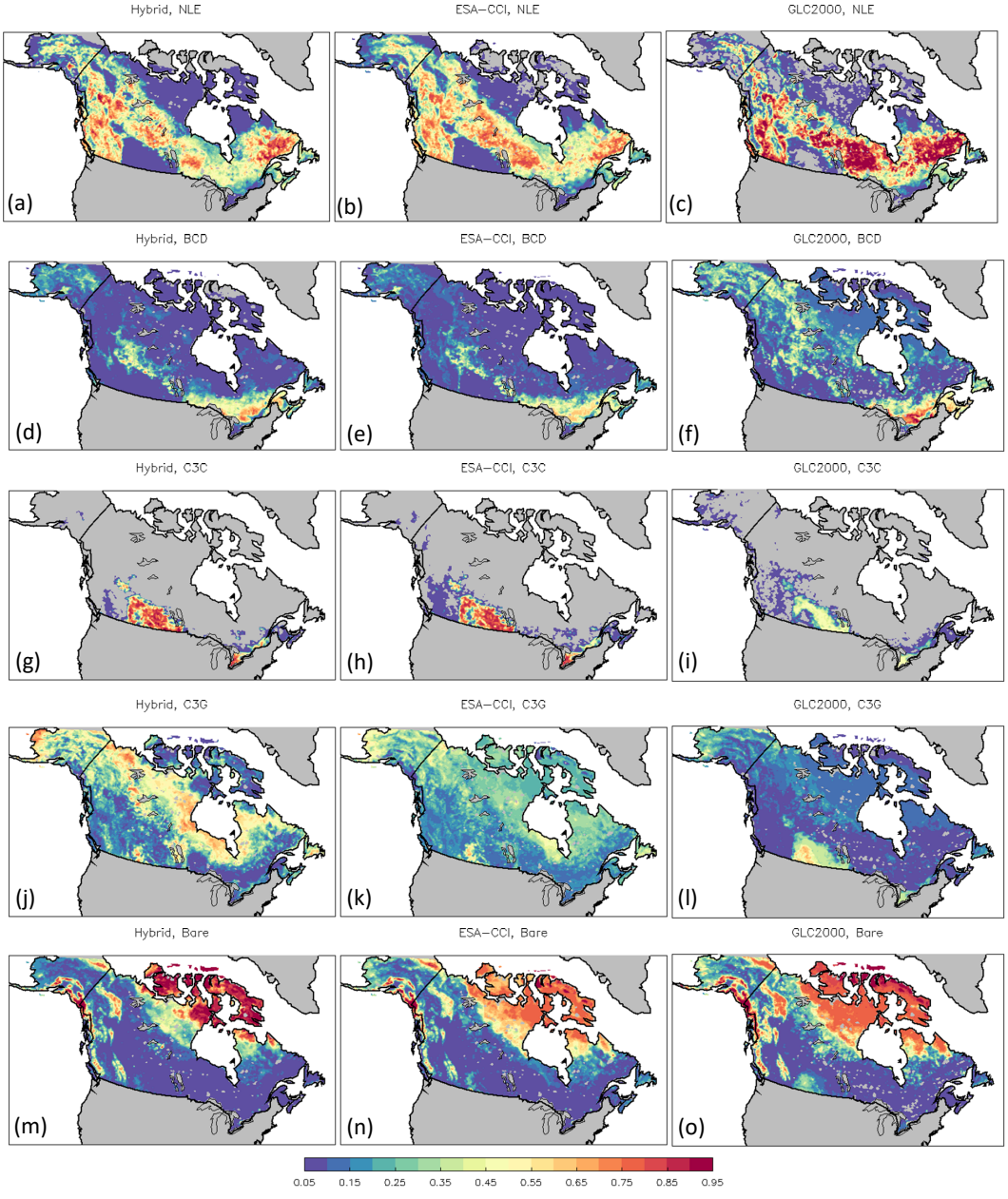

785

786 Figure 3. The spatial distribution of CLASSIC PFTs based on the Hybrid (left), ESA-CCI (middle), and
787 GLC2000 (right) land cover datasets respectively. The maps for C4C and C4G are not shown for their
788 fractions are negligible in Canada. The last panel shows fractions for bare ground from the three datasets.

789

https://doi.org/10.5194/egusphere-2022-923
Preprint. Discussion started: 4 October 2022

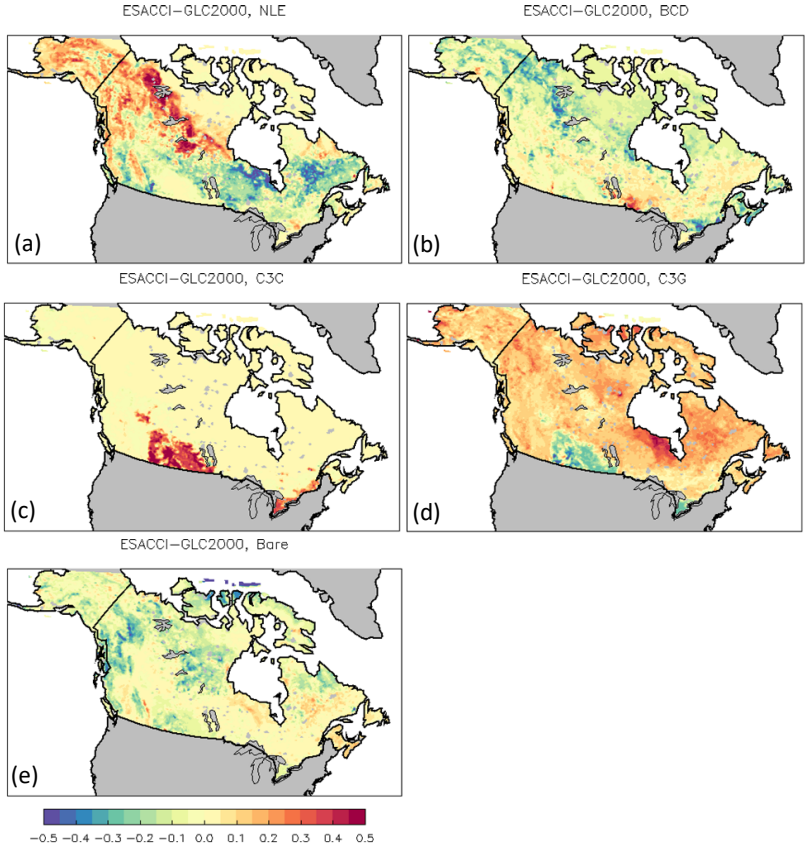

Figure 4. The difference in PFTs based on ESA-CCI and GLC2000 datasets for selected PFTs (a) NLE, (b) BCD, (c) C3C, (d) C3G, and (e) Bare.

https://doi.org/10.5194/egusphere-2022-923
Preprint. Discussion started: 4 October 2022

817

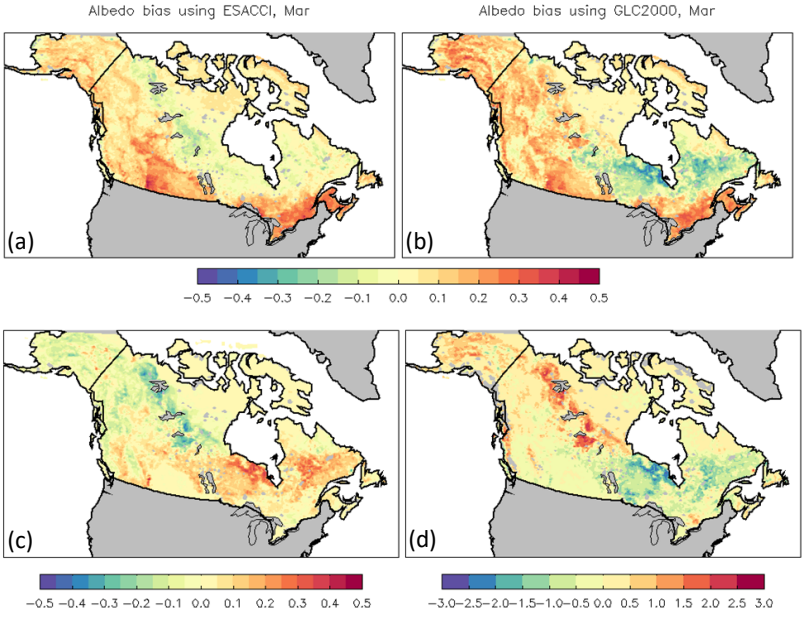

829

830 Figure 5. Surface albedo bias in CLASSIC simulations using PFT distributions based on (a) ESA-CCI,
831 and (b) GLC2000 land cover products. Panels (c) and (d) show the difference in simulated surface albedo
832 (c) and leaf area index (d) between the two simulations.

833